Suvashree Das Int. Journal of Engineering Research and Application *www.ijera.com*
ISSN : 2248-9622, Vol. 8, Issue 9, (Part -1) Sep.2018, pp.148-163

RESEARCH ARTICLE OPEN ACCESS

At wave length coherent scatterometry microscope using high-order harmonics forEUVmaskinspection

Suvashree Das, Prangya Parimita Tappo,
Gandhi Institute of Excellent Technocrats, Bhubaneswar, India
Eastern Academy of Science and Technology ,Bhubaneswar, Odisha, India

ABSTRACT
Inthisreview,wedescribeourresearchonthedevelopmentofthe13.5nmcoherentmicroscopeusinghigh-orderharmonicsforthemaskinspectionofextremeultraviolet(EUV)lithography.EUVlithographyisagame-changingpieceoftechnologyforhigh-volumemanufacturingofcommercialsemiconductors.ManytopmanufacturersapplyEUVtechnologyforfabricatingthemostcriticallayersof7nmchips.Fabricationandinspectionofdefect-freemasks,however,still remaincriticalissuesinEUVtechnology.Thus,inourpursuitforaresolution,wehavedevelopedthecoherentEUVscatterometrymicroscope(CSM)systemwithasynchrotronradiation(SR)sourcetoestablishtheactinicmetrology,alongwithinspectionalgorithms.TheintensityandphaseimagesofpatternedEUVmaskswerereconstructedfromdiffractionpatterns usingptychographyalgorithms.Toexpeditethepracticalapplicationofthe CSM,wehavealsodevelopeda standalone CSM, based on high-order harmonic generation,as an alternativetotheSR-CSM.Sincetheapplicationofacoherent13.5nmharmonicenabledtheproductionofahighcontrastdiffractionpattern,diffractionpatternsofsub-100 nssizedefectsina2Dperiodicpatternmaskcouldbeobserved.Reconstructionofintensityandphaseimagesfromdiffractionpatternswerealsoperformedforaperiodicline-and-spacestructure,anaperiodicangleedgestructure,aswellasacrosspatterninanEUVmask.
Keywords:high-orderharmonics,coherentEUVlight,EUVlithography,coherentEUVscatterometrymicroscope,synchrotronradiation,EUVmaskinspection
(Somefiguresmayappearincolouronlyintheonlinejournal)

I. INTRODUCTION

Extreme ultraviolet (EUV) lithography with reflective pho-tomasks is currently being refined for high-volume manu-facturing(HVM) ofchipswithdimensionsof7 nmorless.ASML's NXE scanners are widely utilized by a multitude ofsemiconductor manufacturers. EUV scanners can replace themostcritical(difficultmultiplepatterning)layersandprovide lithographycapabilitiescomplementarytoArFtechnology.

However, the fabrication and inspection of defect-free masksstill remain one of the most critical issues facing EUV tech-nology. Although defects on the mask have been reducedwitheachpassingyear,manufacturingdefect-freeEUVmasksisstillextremelydifficultinpractice.Thedevelopment of inspection tools for EUV mask is paramount to detectingdefectsandthusproducingdefect-freeEUVmasks[1–4].Forthe EUV mask blank inspection, Actinic blank inspection(ABI) tools [5, 6], based on darkfield microscopy, are widelyused.Thissystemsatisfiestherequirementsforhigh-sensitivity and high-speed inspection of printable defects on maskblanks. Additionally, tools with a high magnification reviewmode improve defect position accuracy. As a result, infor-mation about EUV buried defects can be effectively obtainedand analyzed with ABI tools. To mitigate mask defects, apattern shift method has been developed to cover the multi-layer defects under the absorber pattern. Because it is extre-mely difficult to prevent all defects, an EUV actinic reviewtool is essential for the inspection of printable phase defectson the patterned mask. However, there is no commerciallyavailable tool for the accurate determination of the preciseshape of the buried defects on mask blanks or the printabilityof the defects in the patterned mask. Coherent scatterometrymicroscopyisoneofthemostattractivemethodsusedto solve the aforementioned issues [7–11]. The coherent EUVscatterometrymicroscope(CSM)offersreflectionmodecoherent diffractive imaging (CDI) [12]. X-

ray CDI [13–15]with synchrotron radiation (SR) has been widely used forbiologicalandmaterialapplications.TheCDIisalensless
system, where the image-forming optics are replaced by aninverse computation using scattered intensity. CDI is able toretrieve a phase in frequency space to reconstruct an aerialimage.
WehavedevelopedtheCSMsystemwithaSRsourcetoestablishtheactinicmetrologyaswellasinspectionalgorithms[7–11].Wethendemonstratedthereconstructionoftheinten-sityandphaseimagesoftheline-and-spacepatterns(L/S),the crosspattern,andtheprogrammedphasedefect[9,10]. Amicro-CSM[16–19]thatusesaFresnelzoneplate(FZP)tofocusthecoherentEUVlighthasalsobeenconstructedforthepurposeofevaluatingsmallphasedefectsonamaskblank.Observationofactualphasedefectsonamaskblankwasthen demonstrated using this system [12]. This information is crucialwhen pattern-shift is employed as a defect avoidance technique.However,becausetheSRisalarge-scalefacilityanddepletesmost of the flux in obtaining coherent EUV light, it is notpracticalfor real-worldmanufacturingapplications.
High-order harmonics, however, is a promising alter-nativetoSRforatable-topcoherentEUVlightsource[20–23]. We have developed a phase-matched, high-orderharmonicssourcefortheCSM.Inthisstudy,wesuccessfullygeneratedlow-divergence,coherenthigh-orderharmonicsin theEUVregionwithacommercialpumpinglaser[24]. Usingthe high-order harmonic generation (HHG)-CSM system, weobserved programmed pattern defects in a periodic patternedmask.InthediffractionpatternfromtheEUVmask,a2nm
wide line defect in an 88 nm line-and-space pattern as well assub-100nssizedabsorber defectsina112 nmholepattern

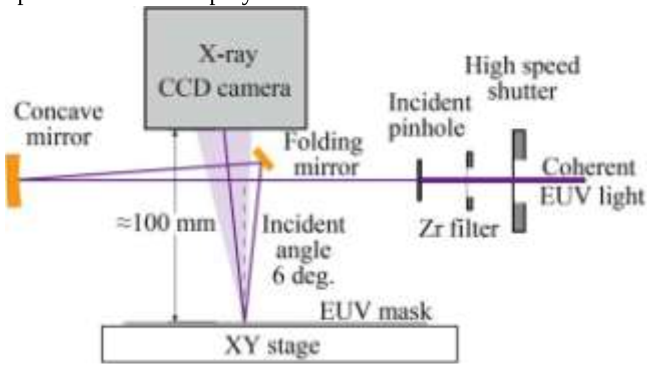

Figure1.SchematicviewoftheCSM.

werebothdetected[25–27].Byfurtherimprovingthesystem,we demonstrated the successful reconstructions of an-88 nmperiodicL/Spatternandacross-patternwithaquantitative
phase contrast [28]. These results signify the that the stan-daloneHHG-CSMsystemhastremendouspotential.

1. KeytechnologiesofCSMsystem

CSM

A schematic view of the CSM is illustrated in figure 1. TheCSM is composed of a concave mirror, a folding mirror, apiezo stage placed on the XY motor stage, an EUV filter, anEUV CCD camera, and a pinhole. These mirrors were coatedwithMo/Simultilayer.Aconcavemirrorplaced onthelinearstage is used to focus coherent EUV light onto the EUVmasks. By using a folding mirror, the incident angle to theEUV mask is set at 6°, which is the same as that of currentEUV lithography scanners. The EUV mask is placed on thestages to scan the observation points. The configuration isoptimized for each coherent EUV light. The EUV mask isthenexposedtoafocusedcoherentEUVlight.Thediffractionpatterns from the EUV mask are subsequently recorded byCCD camera. The surface of the CCD sensor is placed par-allel to the mask surface. Two CCD cameras are exclusivelyused to alter the acceptance angle of the detector. The RoperScientificMTE-2048Bcamerawith2048 × 2048,13.5μmsize pixels is mainly employed as a detector. The EUV CCDcamera is utilized because it can operate in a high-vacuumenvironment.TheCCDcameraiscooledtoatemperatureof −50°C.SincethedistancebetweenthemaskandCCDcameraisabout100 mm,the spatialresolutionislimitedto59 nmbynumericalaperture(N.A.) of0.14.Assignal-to-noise ratio (SNR) is a key performance metric for the CSM,thus,weusedthecamerawith4×4binning,where4× 4 pixels are treated as one pixel during readout. Therefore, thenumber of pixels with the binning condition was 512 × 512.TheSNRhasbeentherebyimprovedbyafactorof4.

CSMequippedwithSR

TheCSMwasinstalledintheBL-3beamlineoftheNewSUBARUsynchrotron radiationfacility, which employs

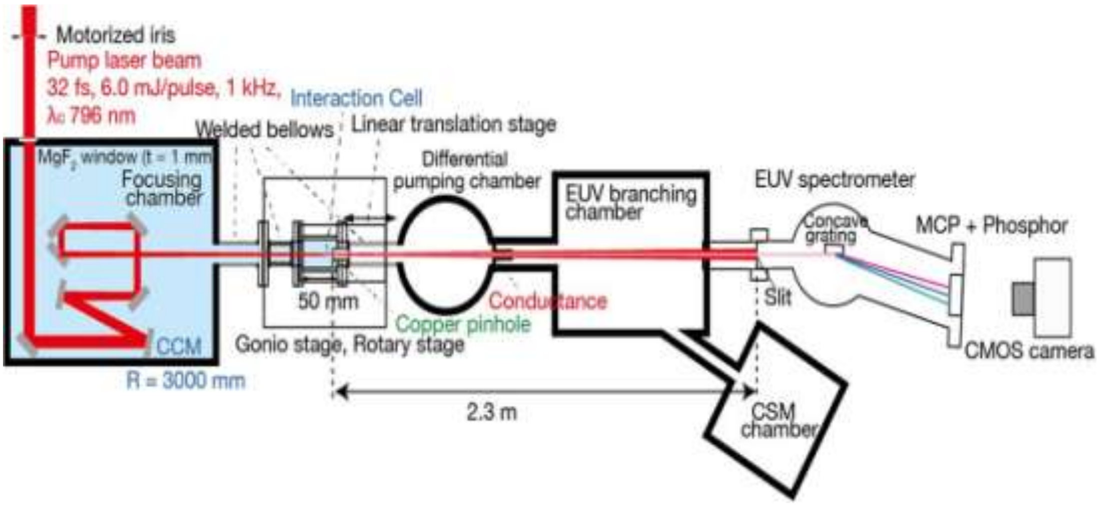

Figure 2.Experimentalsetupforhighorderharmonicgeneration.

abendingmagnetasalightsource[7,8].Twotoroidalmirrors were used to collimate and deliver the SR to a con-cave mirror in the CSM system. Since the SR is partiallycoherent in time and space, a pinhole with a diameter of 5 μmwas exposed to the SR to extract spatially coherent radiation.The pinhole is also used to stabilize the observation point ontheEUVmask.Thelightthatpassedthroughthepinholewasfocused onto the mask via a concave mirror with a curvatureof 200 mm and a folding mirror at equal magnification. ThosemirrorswerecoatedwithaMo/Simultilayerandhasareflection bandwidth of 0.4 nm, which improves the temporalcoherence.Asaresultofthespatialandtemporalfiltering,thecoherent EUV power on the mask was reduced to 1.2 pW.The spatialcoherence length of the incidentbeamis about90μm,asestimatedfromthedivergence.Thisissubstantially largerthantheCSM-fieldsizeof5 μm.Thex–ystagecanshifttheEUVmaskalongthehorizontalplane.Themaximumtravelrangeofthestage is ± 75 mm,forthefull-fieldinspectionofa6″EUVmask.Theminimumstepofthestageis100nm.TwoencodersofMagnescaleLASERSCALE were also monitored during the scan, the minimum step sizeofwhichis34.5nm.

HHGsource

Wehavealsodevelopeda13.5 nmHHGsourceequippedwith acommercialTi:sapphire laser (Spitfire pro 6 W) [24].The laser delivers 1 kHz pulses with durations of 32 fs andenergyupto6.0mJ,atacenterwavelengthof796 nm.Thelaserbeamdiameter($1/e^2$)wasexpandedfromitsoriginal sizeof9.5–12.0mmbyalteringtheconfigurationoftheGalileantypebeamexpander,whichwasplacedbeforethe pulse compressor to reduce self-phase modulation. The lasersystem was installed on the Newport RS 2000 optical table.Figure2displaystheexperimentalsetupforHHG. Amotorized iris diaphragm was placed in the pump laser pathontheendoftheopticaltable.Thepumppulsewasintro-concavemirror.Theangleofincidenceontheconcavemirrorwas optimized to correct the astigmatism of the pump pulse.The measured beam waist was about 90 μm in the vacuum.The maximum focused intensity in the vacuum was 1.1×10^{15} W cm^{-2}. Folding mirrors were then used to directthepumppulseintothecenteroftheentranceslitofanEUV spectrometer, which was also employed to adjust the focalpoint at the end of the interaction cell. The gas-filled regionwas sealed with a Cu foil at the end of the cell and subse-quentlyevacuatedwithadrypumpintoavacuumoflessthan10 Pa. A pinhole was drilled into the Cu foil by the attenuatedpump pulses. The cell was mounted on a translation stage,which was combined with a gonio stage and a rotation stage.The position of the pinhole was then scanned axially alongthe beam. The differential pumping chamber, the branchingchamber, and the EUV spectrometer were all evacuated withturbomolecularpumps.Thespectrometerwasmaintainedata pressurebelow10^{-5}Pa.Thespectrometer,whichwasplaced 2.3mfromtheexitpinhole,iscomposedofagrazingincident flat-field grating and a microchannel plate assembly, coupledwith a phosphor screen and a CMOS camera. In order tooptimize the phase matching conditions for HHG, the targetgas pressure should be adjusted to balance the geometricalphase shift as well as the dipole phase shift. The diameter oftheirisaltersnotonlythegeometricalphaseshift,butalsothepropagation of the intense pump laser pulse in the target gas.Therefore, the high-order harmonic output is extremely sen-sitive to the diameter of the iris. As a result of optimizing thephasematchingconditions,themaximumpulseenergyofthe59thharmonicwasobtainedinheliumatapressureof15kPa,during which the aperture diameter was set to 11.5 mm. Thebeamdivergenceoftheharmonicswasthenmeasuredtobe 0.75 mrad. The spectral width of the 59th harmonic was alsomeasured, resulting in a 0.09 nm full width at half-maximum,whichapproachestheresolutionlimitofthespectrometer.

Figure 3demonstrates the pressure dependence of thehighharmonicspectrum.Atoptimumpressure,theeffective ducedthrougha1mmthickMgF windowintothefocusing interactionintensityestimatedfromthecut-offwavelength

2 14 −2

chamberandwaslooselyfocusedwithanR=3000mm [29]inthespectrum was5×10Wcm.Whenthegas

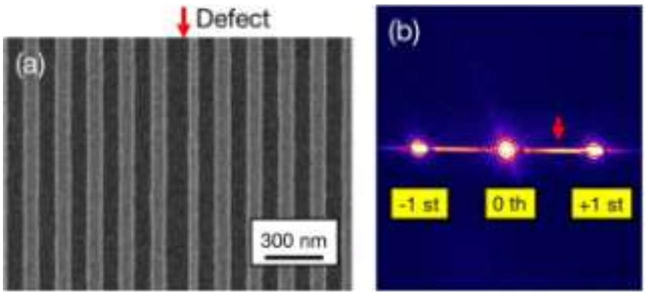

Figure3.Observedhigh-harmonicspectrainhelium.

pressure was increased from 15 to 16 kPa, the output of 59thharmonic decreased by a factor of 5. The results indicate thatthe phase matching conditions have been met, and the tun-nelingionizationdoesnotaffectphasematchingconditionsatthisintensity[30].Thisoutputenergywasapproximatedfrom aphotodiode(IRDSXUV-100)current,whichwasgeneratedfromtwoZrfilters.Sincethecurrentincludednotonlythe 59th harmonic output, but also harmonic outputs of otherorders, the output energy was calibrated by taking the HHGoutputspectrum,photodiodequantumefficiency,andthefilterspectrumintoaccountaswell.Asaresult,a highEUV outputenergyof1nJ/pulse (averagepower:1 μW) wasachieved[25].

Imagereconstructionfromdiffractionpatterns

Thepatternimageswerereconstructedviaptychography[31–33],basedonCDIalgorithms.Thesampleisilluminated with step-and-repeat exposures. Diffraction images are thenrecordedateachstepposition.Thesteplengthshouldbe shorterthanthebeamdiametersuchthatanoverlappedregionis established. Hence, some diffraction images have over-lapped sample information under different illumination con-ditions. The resulting redundancy in the data is essential initerative reconstruction techniques. A sample aerial image isretrievedthroughiterativecalculationsofFourierand inverse-Fourier transforms with constraints. In iterative calculationsusedinptychography,therevisedresultsof thereconstructioncalculation are weighted by the probe amplitude. A nonuni-form probe distribution is necessary for the image recon-structionprocess.Therefore,weusedptychographical coherent diffraction imaging in the CSM, which consists of asmallprobeandalargesample.Additionally,wealsoappliedamodifiedphase-retrievalalgorithmforptychography,whichsimultaneously reconstructs the probe structure of the illu-minatingEUVlightonthesamplewhiletheiterationistakingplace. First, a complex amplitude distribution of an illumi-nation probe was reconstructed using a prior pattern with aknownshapeandstructure.Asampleimagewasthenreconstructedwithouttheprobereconstructionalgorithm.Lastly, the sample image was reconstructed with the probereconstructionalgorithm.

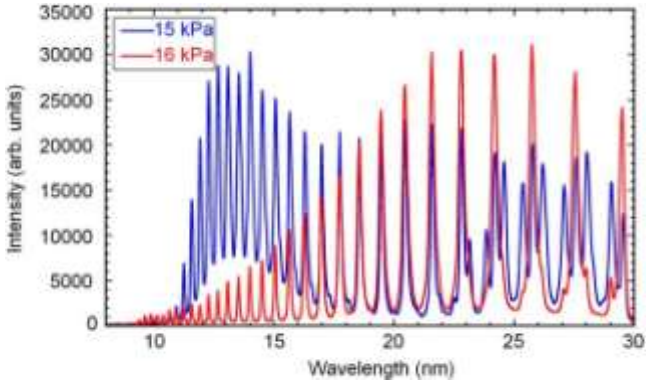

Figure 4.(a) SEM image and (b) diffraction pattern of a line-defectin88nmL/Spattern.Reproducedwithpermissionfrom[9].©2011AmericanVacuumSociety.

2. SR-CSMsystem

We observed an amplitude defect in the absorber patternsusing the SR-CSM system. Figure 4(a) displays the SEMimage of the defect, which is a line defect in an 88 nm L/Spattern[9].Thedefectlineis30nmmorenarrowthanthe otherlines.Thedefectlinewidthvariedfrom2to40nm,and thelinewidthoftheabsorberrangedfrom44to86 nm.Figure4(b)showsthediffractionpatternresultingfromthe defectaswellastheL/Spatterns.Theexposuretimewas 100s.Diffractionfromthedefectwasclearlycapturedasaline diffraction pattern in the transverse direction. As thedefectlinewidthwasreduced,abroaddiffractionpatternspread out on both sides of the 0th order maximum in thetransversedirection.Thedefectsignalsignifyingadefectsizeofup to 10 nm inwidth was detected inthe diffractionpat-tern. Thus, the CSM is able to detect the defect as the dif-ference within the observed diffraction pattern without theneed to reconstruct the aerial image. This CSM inspectionusing the diffraction pattern also has the advantage of theability to rapidly detect the existence of defects in the field ofview. Nonetheless, image reconstruction is still essential fordetecting the defect position. Theoretical detection limits forthe defect sizes depend on the SNR of the detector noise, thesource brightness, and the substrate roughness. The substrateroughnessgeneratesspecklenoiseontothesignal.Ifthedetectornoiseisatanimaginaryzero,thenthedetectionlimitisestimatedtoapproximately30 nmintheL/Spat-ternedmask.

Figure 5(a) exhibits the image reconstruction result of thedefectviaptychographicalCDI.Thedefectwasilluminatedat7× 2 points with a 1 μm step [9]. A bright line resultsfromthe defect in the L/S pattern. However, the periodic L/Spattern around the defect produces a blurred shape due to thenoiseintheimagereconstruction.Wefilteredoutthe dif-fraction from the periodic L/S signal and reconstructed theaerial image, as shown in figure 5(b). The defect was clearlydetectedwithoutaperiodicstructure.Thus,theCSMcan effectivelyinspectthedefectpositionsthroughtheapplicationofptychographicalCDI.

Figure6displaysacomplexamplitudeimagewithamplituderepresentedbybrightnessandphaserepresentedby hue [10]. The sample pattern used was a crossed lines patternwithawidthof2μmandalengthof10 μm,wheretheshape

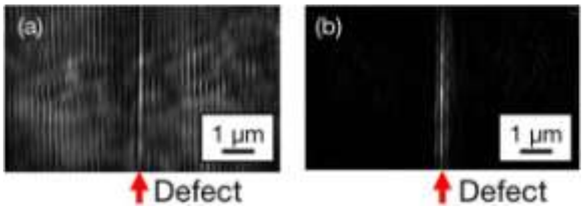

Figure 5.(a)Reconstructionimageofline-defectand(b) thatwiththeperiodicsignalfilteredout.Reproducedwithpermissionfrom[9].©2011AmericanVacuumSociety.

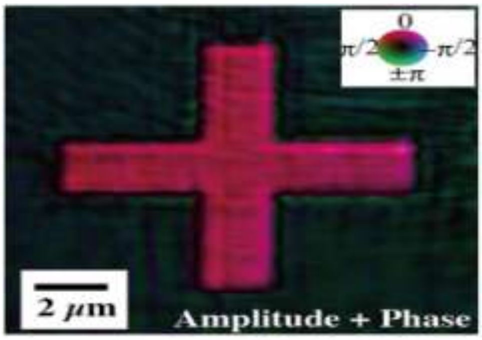

Figure6.Complexamplitudeimageofcrossedlinepatternwiththeamplituderepresentedbybrightnessandthephaserepr esentedbyhue.Reproducedfrom[10].Copyright©2013TheJapanSocietyofAppliedPhysics.Allrightsreserved.

was already known. Thirty-six diffraction patterns were usedforthereconstruction.Thesamplingpositionwass hiftedin2 μm steps, overlapping its 5 μm diameter with the probe. Thecross shape was well-reconstructed with symmetrical results.Aspreviouslydescribed,CDIretrievesthephas einfrequencyspace to reconstruct the image. Therefore, the phase data ofthe aerial image in real space can be simultaneously recon-structed. The red region of the crossed line corresponds withthe reflective multilayer region, and the dark green regioncorresponds with the absorber region. The phase differencebetween the absorber and reflection regions was found to beapproximately145°.Theabsorberregionhasamorea dvancedphasecomparedtothereflectionregion,simila rtoabumpstructure,becausetherefractiveindexofthea bsorberislessthan1.Thecalculatedphaseshiftisapprox imately140°,comprising of an absorber structure with a 10 nm thick CrNbufferlayeranda51nmthickTa-basedabsorber,whichisinlinewiththeexperimentalva lues.Thereflectivityoftheabsorberregionwaslessthan 2%,whilethatofthemultilayerregionwas62%.Althou ghthereflectivityoftheabsorberwas31 times less than that of the reflection region, the absorberregion information was not limited. The CSM records theinterference of the reflection amplitude and found that thereflectionamplitudesoftheabsorberandthemultila yerswere 0.14 and 0.79, respectively. For example, when the absorbertomultilayerregionratiois1:1intheilluminati onprobefield,

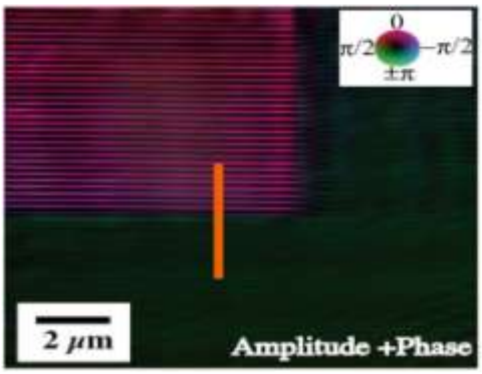

Figure 7.Complex amplitude images of a corner part of 88 nm L/S.The amplitude represented by brightness and the phase representedbyhuepattern.Reproducedfrom[10].Copyright©2013TheJapanSocietyofAppliedPhysics.Allrightsrese

rved.

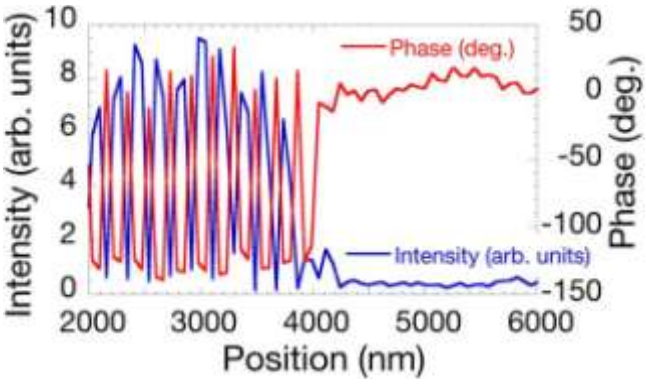

Figure8.Profilesofintensityandphaseatthepositionindicatedbytheorangelineinfigure7.Adaptedfrom[10].Copyright ©2013TheJapanSocietyofAppliedPhysics.Allrightsreserved.

thecontrastoftheinterferencefringeissufficientlyhigh at 0.34.Thus,theCSMsystemisadeptatprovidingtheabsorberregioninformation.

Figure 7presents the reconstructed complex amplitudeimages of a corner structure of an 88 nm L/S pattern, which islocated on the same mask as the crossed line pattern [10]. 25diffraction patterns were used for the reconstruction process.Thepositionofthesamplewasshiftedin1.5µmsteps.TheL/S structure and the corner structure were both successfullyreconstructed.Figure8detailstheintensityandphaseprofilesat the position indicated by the orange line in figure 7. Thephase difference between the absorber and the multilayerregionisapproximately145°,whichisidenticaltothereconstructed absorber phase shift shown in figure 8[10].This demonstrates that CSM can accurately and thoroughlyevaluate the phase profile of the L/S pattern. These resultsclearly display that CSM is proficient at evaluating phasedefects. When this system was put in practice, a programmedphase defect was evaluated successfully [10]. This techniquehasalsobeenextendedtoamicro-CSMsystemandwasonceagainsuccessfulintheevaluationofnativephasedefects.

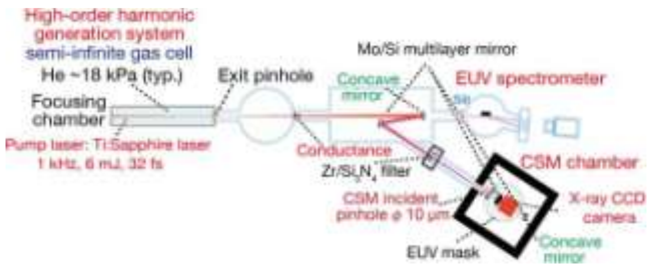

Figure9.OpticaldoublerelaysystemforHHG-CSMsystem.

3. HHG-CSMsystem

Experimentalsetup

The configuration of the CSM is very similar to that of theSR-CSM system. Phase-matched high harmonics is used as acoherent EUV light. The beam divergence of the 59th har-monic was measured to be 0.75 mrad. Assuming that theharmonics is a Gaussian beam, the beam size at the exitpinhole is estimated to be 5.7 µm. The setup of the opticalrelay system is illustrated in figure 9 [25]. High harmonics isrelayedontoanincidentpinholeintheCSMchamberusingaremovableconcavemirrorwitharadiusofcurvature of2.0m,as well as a flat mirror placed in the branching chamber.Those mirrors were coated with a Mo/Si multilayer whichhas a reflective bandwidth of approximately 0.4 nm near thewavelengthof13.5 nm.The59thharmonicwasselectivelyreflected and the magnification of the relay optics was 1.0.The Zr filter was placed between the branching chamber andtheCSMchambertoremovethepumppulse,roomlight,andout-of-bandradiation.TheZrfilterisafree-standingmem-brane,witha200nmthickZrlayeranda50nmthickSiN currentnoise.Toachievehigherspatialresolution,wedeveloped a state-of-the-art CCD camera with a large CCDimagesensor(e2vtechnologiesCCD230-84)of61.4×61.4 mm^2[25].Thenumberofpixelsis4096×4096andthe pixel size is 15 × 15 μm^2. The imaging area was then cooleddown to a low temperature of −40 °C using a Peltier device.Accordingly,alowdarkcurrentnoiseof0.02electron/s/ pixel was achieved. The NA is a function of sensor size anddistance from the mask to the sensor, which is directly pro-portional to size and inversely proportional to distance. Sincedistance is restricted by both optics size and oversamplingconstraint, the camera recorded a high NA of 0.31 at thedistanceof95mm.Thespatialresolutionwasthusenhancedto27nm.

CoherenceevaluationofHHG

Whenthefirstexperimentwas conducted to analyzethespatialandtemporalcoherenceoftheharmonics,a112nmL/Spatternwasusedtogeneratehigh-ordermaximain the sensor [25]. The coherent length of the harmonics iscalculatedto be1.0 μm, whilethemaximumpath differenceat the sensor is calculated to be 3.0 μm. Although a full-fieldimagewasdifficulttoachievewiththissetup,there were10 other diffractions (±1st- to ±5th-order diffractions) in addi-tiontothe0th-orderdiffraction.Thus,theHHGEUVsource demonstrated successful observation of the EUV mask. ThenewCCDcamerarecordedanextensiveimagingarea,includingdiffractionsup tothe 5thorder.Figure 10(a)showsa diffraction pattern with a 2 nm wide line defect in an 88 nmL/Spattern,wheretheimagecontrastisadjustedtohighlighttheweakdefectsignal[25].Asindicatedbythearrows,the

3 4

linediffractionsignalfromthenarrowlinedefect,whichis support layer. Since this tensioned filter has no wrinkles, thehigh spatial coherence will not be degraded. The 59th har-monicthatpassedthroughthepinholewasrelayedontothe maskwithamagnificationof1 × usingboththeconcavemirror and the folding mirror (optical double relay system).Thediameteroftheincidentpinholeis10μmwhichis approximately twice the minimum spot size of the 59th har-monic. The role of the pinhole is three-fold: (1) stabilizationof observation point on the mask, (2) spatial filter to extracthighly spatial coherent light from the 59th harmonic, and (3)spatialreductionfilterforthepumppulse.Number3iscrucial to the safe operation of the system. Since the intense pumppulse co-propagates with the harmonics, without a pinhole, iftheZrfilterwasaccidentallydamaged(suchasbypump pulse,differential pressure,etc),themaskwouldbedamaged bythepumppulseaswell.

The large CCD image sensor is the most critical comp-onent of the CSM system used to directly record diffraction.Thespatialresolutionisdependentontheimagingareasizeofthe CCD chip. Hence, a larger detector can record the dif-fraction pattern from a larger diffraction angle, which canprovide higher-spatial-frequency information on the absorberpatternshape.IntheHHG-CSMsystem,aCCDcameraoperateinavacuumduetotheopticslayout,andthechip mustbecooleddownto−40°Cinordertoreducedark not recorded in a defect-free region, is recorded here. Thedefect signal profile is illustrated in figure 10(c), the area ofwhich is indicated by the red line. The signal profile displaystheverticalsignaldistribution,whereaveraginginthehor-izontal direction is applied to reduce signal fluctuation. Thedefect signal is approximately 26 counts, where the back-ground noise signal is approximately six counts. Therefore,the 2 nm wide defect is able to be clearly shown. Compared toprevious results that used the SR light source, the HHG EUVsource has a detection limit that is five times more narrow.Althoughthedetectionlimitisinfluencedbymultiplefactors,the results evidently demonstrates that the spatial coherent ofthe 59th harmonic is high enough to observe defects on thenm-scale.

Beampointingstabilization

The beam pointing stability is one of the most critical issuesfacingtheHHG-CSM.Additionally,thebeamsizeneedstobesmall enough to achieve high resolution in the CSM. In theaforementionedexperiment,thediameteroftheEUVlightonthe mask is approximately the same as that of the incidentpinhole in the CSM chamber. Although the use of a smallpinhole can reduce the beam size, it can also reduce the utili-zationefficiencyoftheEUVlight.Furthermore,abeam

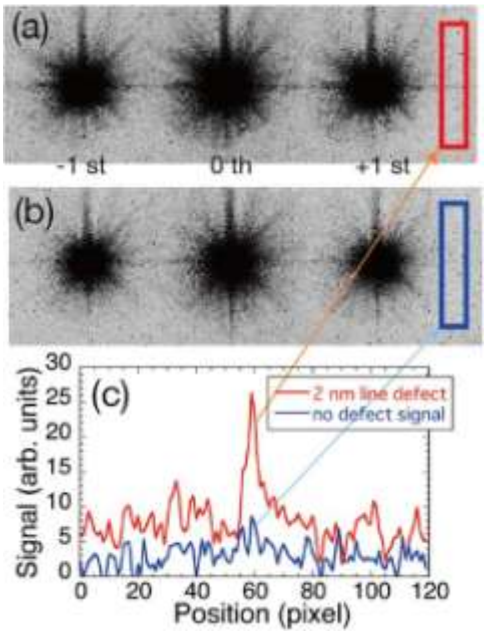

Figure10.(a),(b)Observeddiffractionpatternsfroman88nmL/Spattern,and(c)spatialprofileofdefectsignal.Reproducedfrom[25].Copyright©2012TheJapanSocietyofAppliedPhysics.All rightsreserved.

fluctuationlargerthanthatoftheincidentpinholediametersizeis detrimental to the effective application of high harmoniclight.WhentheEUVlightattheexitpinholeisdirectlyrelayedwiththeconcavemirrorintheCSMchamber,theEUVlightisde-magnified by a factor of less than 1/10. In this case, thebeam-pointingfluctuationsshouldbesmallerthanthebeam size. The beam fluctuations of the pump beam was measuredfor a duration of 20 min at the focus, at ±23 μm (6.7 μmrms)and±24 μm(7.2 μmrms)inthehorizontalandverticaldirectionsrespectively.Relayopticswouldfurtherincrease beam fluctuations. Therefore, we installed a commercial pro-duct called ‘Aligna: Automated Laser Beam Alignment andStabilizationSystem’intheHHGsource. Theexperimentalsetupisshowninfigure11[27].The system is composed of feedback control electronics, a com-binedangleandpositiondetector(PSD),andtwopiezo-drivenmirrors.Abeamtransmittedthroughadielectric mirrorwas used as a reference beam for the beam stabilizer. A turningmirrorthendirectsthebeamtothePSD2.Avariableattenuator and a beam splitter, which direct the beam to thePSD 1, are both placed in the optical path. The PSD 1 ispositioned at the focal point of the reference beam. The dis-tancebetweentheBStothePSD2isapproximately40cm.The power of the reference beam is at least 10 times strongerthantheupperlimitoftheoperationpowerofthe PSD.Duringthis experiment, the interaction cell was removed from thefocusing chamber and a viewport flange was mounted on theexit port of the pump pulse. A CMOS camera was positioned atthe focus to monitor the fluctuation of the pump pulse. Thefocusingchamberwassubsequentlyfilledwithheliumgasatapressureof17kPa.Thepumppulsewasthenattenuatedbeforetheviewportwithadielectricmultilayer mirror.Figure12 displaystheX–Yplotsofthebeampositionsobservedovera

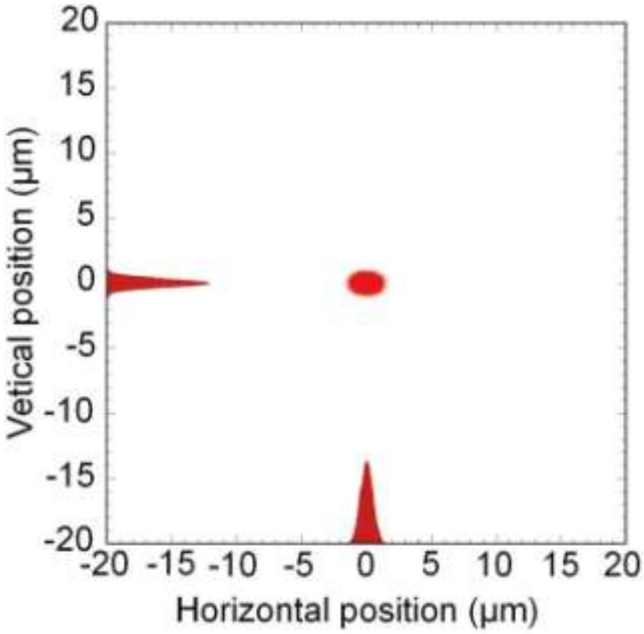

Figure 11.Schematicoftheexperimentalsetupforbeamstabilization.

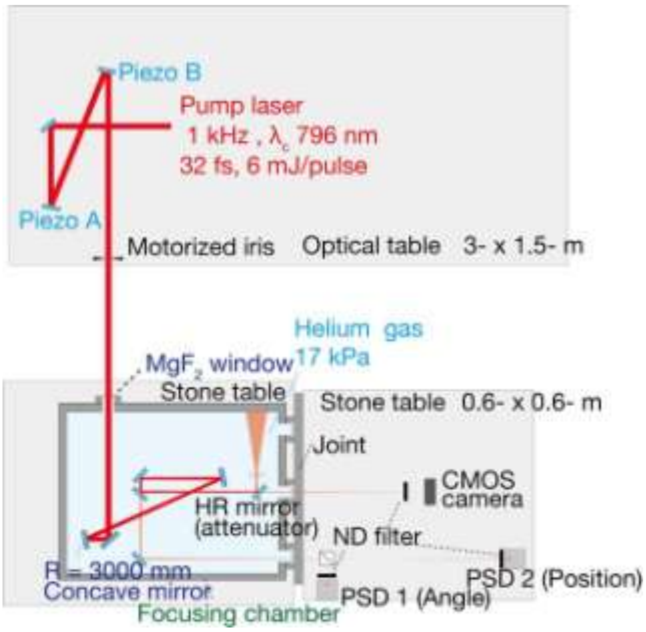

Figure12.X–Yplotsandhistogramofthebeampositionofpumppulseobservedatfocus.

1 hperiodattheCMOScamera.Theplotsshowthatthefluctuation of the pump beam position has been markedlyreducedto0.3µmrms(vertical)and0.5µmrms(horizontal).

Upgradeofopticalrelay system

Thebeampointingfluctuationofthepumppulsewasreducedto much less than that of the 59th harmonic beam size. Sincetheremovaloftheincidentpinholeswasmadepossibleinthe CSMchamber,wewereabletoenhancetherelayopticstoa

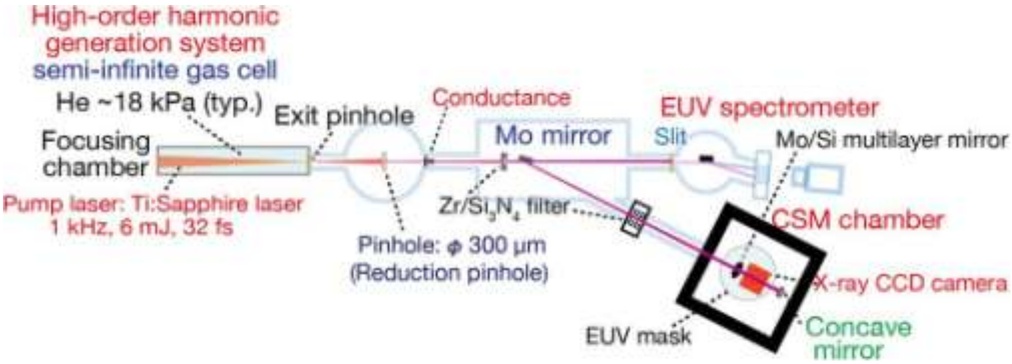

Figure13.UpgradedopticalrelayfortheHHG-CSMsystem.

single optical relay that can directly transfer the 59th har-monic beam to a mask. Instead of the incident pinhole, areduction pinhole with a diameter of 300 μm was positionedinside the differential chamber for the purpose of spatial fil-teringthepumppulseandextractingthehighlycoherent EUVlight [27]. The power of pump pulse was reduced by a factorof 100 by the pinhole. The transmitted EUV light was thendirected to a concave mirror in the CSM chamber with amirrorcoatedwithmolybdenumthin-film.Theangleofincidence on the mirror was 75°. The pump pulse power wasfurtherreducedbyafactorof10afterreflectingofftheirror,sincethemirrorservesasaBrewsterplateforthepumppulse[34, 35]. The curvature radius of the concave mirror in theCSM chamber is approximately350 mm.The distance fromthe EUV source to the focusing mirror and from the focusingmirror to the mask were 3.1 m and 185 mm, respectively. Themagnification of the relay optics was approximately 1/17.Consequently, the utilization efficiency of the EUV light onthe mask was improved 130 fold via beam pointing stabili-zation.Theexperimentalsetupisillustratedinfigure13.

Observationofdiffractionpatternofprogrammed (absorber)defect

Whena2DperiodicholepatternmaskisexposedtoacoherentEUVlightundertheassumptionthatthebeamdiameterismuchlargerthantheperiodofthepattern,intenseinterference maxima is expected appear in the diffractionpattern. In other words, in any location besides the inter-ferencemaxima,theinterferenceisalmostdestructive. Alternatively, if there exists a defect in the exposure area, adiffractionpatternwouldalsobegenerated.Inthedestructiveinterference area, the diffraction pattern originated from theappearance of the defect. When such a diffraction pattern isobserved,theshapeofthedefectcanbeapproximated. Inthisexperiment, a peak intensity ratio of two diffraction patternsresultingfromaperiodicpatternandadefectwascon-siderablywiderthanthedynamicrangeoftheCCDcamera. Toenabletheobservationofadefect's diffractionpattern,thedefectsignalneedstobehigherthanboththetotalintegrated noise and the total diffraction pattern originated from theincoherent portion of the EUV light. Under such conditions,theresultinginterferencemaximumwasmuchhigherthanthesaturationlevelofthesensor,whilebloomingandsmeareffects also appeared in the diffraction pattern. A 0.8 mmdiameterpinholewasinstalledbetweenthefolding mirrorandtheEUVmaskinordertoreducescatteringfromtheoptical element [27]. The focused beam radius ($1/e^2$ radius) on themaskwasmeasuredtobe3.9μm,usingknifeedgemethod.

We observed the EUV mask with hole patterns, which wasfabricated in a square region measuring 25 × 25 μm^2, using aprogrammedabsorberdefectinthecenter.A10×21regionof the hole in a block contained 10 defect shapes and 21defect sizes. The block was surrounded with an absorber linethatis10μmwide.Weobservedtwoholeblocks(112and 180nmindiameter),wherebothhada1:1ratioofholetospacewidth.Sincethemagnificationoftheexposuretoolfor EUV lithography is 1:4, the hole diameters correspond to 28and45nm,respectively,onawaferplane.

Figure 14(a) shows the difference image resulting fromtwo diffraction patterns developed from defective (with 40nm oversize defect) and defect-free areas in the 180 nm holepattern [27]. The Gaussian blur filter is used to smooth theimage,where the exposure timewas 1 s.Figure 14(b) displaya scanning electron microscopy (SEM) image of the defectivearea and corresponding defect shape, which are representedby the solid-orange region. As presented in figure 14(b), theshapeoftheholeandoversizeddefectisclosertothat ofa rounded square than a circle. The defect shape is the same asthatoftheregionboundedbytwoconcentricroundedsquares. In the SEM image, a fringe pattern appears aroundthe central maximum in both vertical and horizontal direc-tions. The 1st and 2nd dark fringes are clearly observed. Thedistance between the dark fringes and intensity ratio of the0th, 1st, 2nd fringes are accurately replicated by the calcul-ationresults.Whendouble-relayopticswasemployedtodetect the same defect, the required exposure time was 1000 s.Thissystemreducedtheexposuretimedramaticallyto only 1s.Figure15(a)exhibitstheSEMimageofthedefectiveareainthe180nmholepattern,aswellasthedifferenceimage resulting from the two diffraction patterns produced by thedefective and defect-free areas, respectively [27]. The solid-greenregioninfigure15(a)representstheshapeofthedefect (no-holedefect).Thediffractionpatternfromno-holedefect is illustrated in figure 15(b). This pattern is identical to thediffractionpatternfromasinglehole.Sincetheintensity distributionoftheinterferencefringesbecomeclosetothatoftheAiry-disc,theintensityofthe1stbrightfringeislessthan

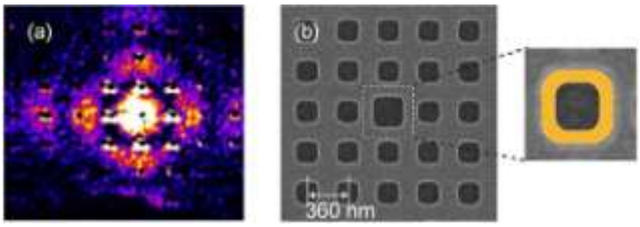

Figure14.(a)Diffractionpatternand(b)SEMimage.

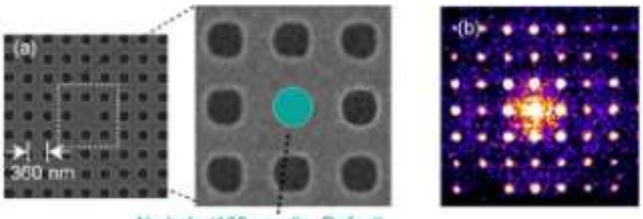

Figure 15.(a)SEMimageand(b)diffractionpatternofnoholedefectin180nmholepattern.

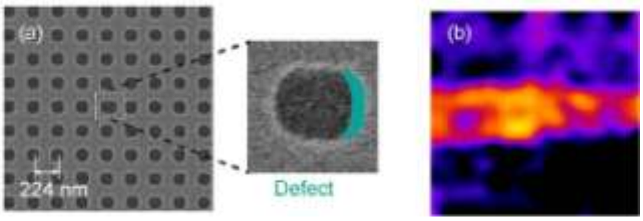

Figure16.(a)SEMimageand(b)diffractionpatternfromline-endoversizedefectin112nmholepattern.

1/20 of that of the central bright fringe. Thus, the 1st darkfringe is barely noticeable, and the hole diameter calculatedfromthediameterofthe1stdarkfringeis200nm.

Figure 16 reveals the SEM images of the line-end 24 nmoversized defect as well as the diffraction pattern resultingfrom the line-end 24 nm oversized defect in the 112 nm holepattern,respectively[27].Thisimageisobtainedusingthe followingprocedures(batchprocessing):(1) priortothecreationofadifferenceimage,aGaussianblurfilterisapplied to each diffractionpattern with a radius of 1 pixel. Thisprocessing is crucial to the reduction of camera noise in adifference image. When this processing is applied to the darkframeofthecamera,atotalnoisecountinthedifference

images of each dark frame is reduced by a factor of 3;
(2)outliersareremovedfromthedifferenceimagesandreplacedby the mean value of the periphery areas; and (3) the Gaus-sianblurfilterisappliedtosmoothouttheimage.Inthe diffraction pattern resulting from a line-end 24 nm oversizeddefect, an averaged signal (count) is only three.
Nonetheless,theshapeofthediffractionpatternisaccuratelyreplicatedby thecalculation.Theresultsuggeststhattheincoherentportionof the EUV light does not affect the observation of smallsignals. We observed these defects using the line step-and-scan method. A defect can be detected with 1 µm steps in asingledirection,scanningfromoneedgetotheotherof ahole

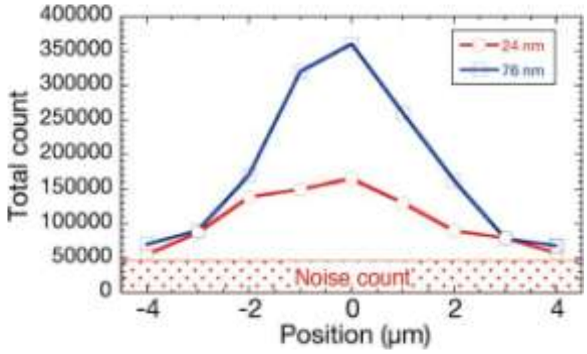

Figure 17.Total count of the defect signal from extended defect viastep-scanmeasurements.

region(25µmlength).Thefluctuationofthediffraction signalintensityis1.8%(1σ)over10min.
Figure17illustratestherelationshipbetweenthepositio n ofthedefectandtheintegratedtotalcountofthedefectsignalresulting from 24 and 76 nm line end oversized defects. Thetotal count of defect signals is calculated via the aforemen-tioned batch processing method. The background noise con-sists of the CCD camera and EUV mask noise. The CCDcameranoisesareresultsfromdarkcurrentandreadoutnoises.EUV mask noises are induced by the roughness of the multi-layer and the absorber. The integrated defect signal for eachdefectshapeisalmostproportionaltothedefectareasizeandthe illumination power. In this study, the shape of the defectscan be deduced from the diffraction pattern without recon-struction of the image. Specifically, when the interferencefringe appears, a more detailed shape can be approximated.Obviously,thediffractionpatterndoesnotincludethepositioninformationofthedefect,thoughtheapproximatepositioncanbedeterminedbyastep-scanmeasurement.Adiffractionpat-ternbegeneratednotonlyfromapatterndefectbutalsofromaphasedefect.Ifaphasedefectexistsundertheholepattern,thediffraction pattern of the phase defect can be identified. Thedetection limit is a line-end 24 nm oversized defect with a 10 sexposure time, which has an area of 2688 nm^2. This area isequivalent to that of a52 × 52 nm^2 absorber defect.Theseresultsindicatethatthespatialcoherenceofthe59thharmonicis high enough to observe such a small signal within a highcontrastsignal.Thedetectionlimitofthedefectsizeisroughlyproportional to the illumination size. Thus, reduction of theilluminationsizewilldramaticallyimprovethedetectionlimit.However, reconstruction of complex images is required toobtaindetailedcharacteristicsofthedefect.

Reconstruction of absorber patterns from diffractionpatterns

In order to reconstruct the EUV mask pattern through pty-chography, diffraction images were obtained via step-and-repeatmeasurement.Ultra-precisesamplestagepositioningisrequiredtoreconstructtheimages.Similarly,thebeampointing and beam profile needs to be stable. In the aboveexperiment,thereductionpinholewasfabricated witha

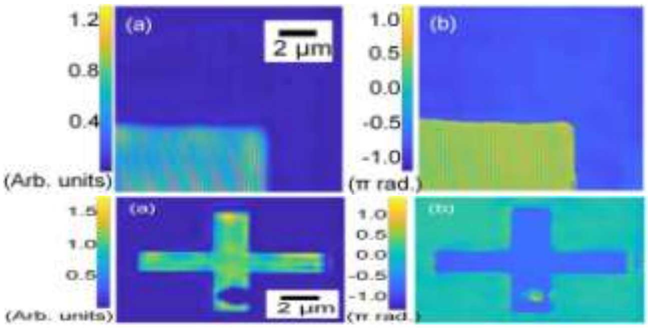

Figure18.Reconstructedresultsof thecornerstructureofthe 88nmL/Spatternintermsof(a)intensityand(b)phase.Adaptedfrom[28].Copyright©2017TheJapanSocietyofApplied Physics.Allrightsreserved.

Figure19.Reconstructedresultsofthecross-linepatternintermsof (a) intensity and (b) phase contrast. Native defect on the cross-line isalsoreconstructed.Adaptedfrom[28].Copyright©2017TheJapanSocietyofAppliedPhysics.Allrightsreserved.

SUS304steelplateof1 mmthickness[28].However,thepinhole was deformed due to heat produced by the high-power pump laser beam. The deformation of the pinhole thusaffected the beam quality of the 59th harmonic. Therefore,reconstructing the EUV mask pattern was challenging. ToimprovethestabilityoftheEUVlightspatialprofile,a tungstenpinholewithhighthermalresistancewasused. The thickness of this tungsten pinhole was the same as that of theSUS304pinhole(1 mm).Themeltingpointoftungstenis3,420 °C,whichis2.4timeshigherthanthatofSUS304(1400 °C).Thus,the1/e^2spotradiusofthefocusedEUVlight,measuredusingtheknifeedgescanmethod,was reducedto1.6μm. Forhigh-precisionsamplepositioning,apiezoflexurexystage (Piezosystem Jena PXY 200SG) was installed onto thepulse motor stage, which had an integrated strain gauge forpositionfeedback.Thestrokelengthis160μminthex-andy-directions.Theresolutionis4 nmandtherepeatabilityis45 nm. The accuracy of the mask stage position for ptycho-graphywassignificantlyimprovedwiththissetup.Toestablishanaccuratecomparison,thisexperimentusedthesamesampleasbefore.Twotypesofabsorberpatternswereobserved.Oneisan88nmL/Spattern,designedinasquareregionwithan areaof25×25μm^2.Itsline-to-spaceratiois1–1.Theotheris acrossline-patternwithawidthof2μmandlengthof10μm. Diffraction patterns from the cross-line pattern and the 88 nmL/S pattern were recorded by the CCD camera. The mea-surement was conducted at 15 × 15 points for step-and-repeatmeasurements. The exposure time was 0.3 s at each point andthe readout time of the CCD camera was 4.5 s per image. Thetotal observation time was 17 min at 15 × 15 points, where thereadout time was dominant to the observation time. Since thespatial profile stability of the HHG EUV source was greatlyimprovedbythetungstenreductionpinhole,diffractionsfromthepatternwere clearlyrecorded.Figure 18displaysarecon-structedimageofthecornerstructureofthe88nmL/Spattern [28],wherefigure18(a)showstheintensityimageand figure 18(b) exhibits the phase image. As revealed in figure 18,thelineandcornerstructuresarewell-reconstructed.Addi-tionally, the phase image demonstrates that the phase mod-ulation of the line pattern is clearly observed. Thus, the CSMcanclearlyandaccuratelyobservetheabsorberpatternphase,whichiscriticalinpredictingthemask-inducedaberration.

Figure 19 illustrates a reconstructed image of the cross-linepattern[28].Theintensityimageisshowninfigure19(a)andthe phase image in figure 19(b). The cross structure shown hereisalsowell-reconstructed.Thereconstructedimagequality resulting from the HHG-CSM is higher than that resulting fromthe SR-CSM (figures 6 and 7) since both the EUV light powerand position accuracy was significantly improved. Using thephase image, we were able to estimate the phase shift of theabsorberpattern.Thecross-lineregionisthe reflective multi-layer without the absorber. The outer region of the crossstructure was covered by the absorber layer.

The differencebetweentheabsorberandreflectiveregionswasestimatedtobe 2.8 rad (160°). The CSM can estimate the absorber phase shift,whichisessentialtoachievingtheattenuatedphase-shiftmask[36–39]. In addition to the cross pattern, a natural defect thatappearstobeaparticleof∼2 μmonthepatternwasalsoobserved.Thephaseshiftoftheparticlewasthesameasthatof the absorber pattern, which indicated that this particle is apeeledabsorber.Asshown,thephaseshiftisextremely advantageous for characterizing the defect origin. Hence, phaseinformationisessentialforachievinganaccurateandthoroughinspectionofthemask.

4. AdvancedHHG-CSMsystem

For the inspection of printable defects, the probe beam sizeshould be less than ∼100 nm. An FZP is a key optical elementfor focusing of high harmonics on the sub-μm scale. An off-axisshortfocallengthzoneplatecanbeintegratedintoanEUVmaskscanningmicroscopeequippedwithanHHGsource[40–42].Alowerdivergencebeamisrequiredtoincreasethecouplingefficiencybetweenan EUVlightandanFZP. With a lower divergence, a Gaussian profile harmonicemissionwith a divergenceof0.18mrad($1/e^2$)wasobtained underanotherphasematchingconditioninhelium.The beam divergenceofthe59thharmonicisapproximately1/20ofthatof the pump pulse. Thus, the majority of the low divergencebeam can pass through the reduction pinhole. Compared topreviousresults,thoughthepulseenergyofthe59thharmonic is about 1/3, the fluence of the harmonic is ∼5 times higher.Therefore,theadvantageofthelowdivergencebeamisthe ability to not only improve spatial coherence, but also theutilizationefficiencyoftheHHG-CSM systemharmonic. Consequently, the illumination power on the mask is increased.The beam radius of 24 μm at the exit pinhole, estimated by therelationship between the beam waist and the divergence ofGaussianbeam,ismuchlargerthanthepointingfluctuationsofthepumppulse.ThepointingstabilityoftheEUVlightonthemaskwillbefurtherimprovedbyapplyingthelowdivergencebeam.Combiningthelowerdivergencecoherenthighharmo-nicbeamwithFZPtechnologieswillsignificantlyimprovetheresolutionlimitoftheHHG-CSMsystem.

II. CONCLUSION

We have developed a CSM system using a SR source toestablish actinic metrology and inspection algorithms. Thediffraction patterns of an 88 nm L/S pattern and crossed-likepattern with a width of 2 μm on the EUV mask were observedusing the SR-CSM system. The complex images of the maskpatternswereaccuratelyreconstructedfromtheobservedimages through applying the modified phase retrieval algo-rithm. The results demonstrate that the SR-CSM system canevaluate absorber phase shift values qualitatively. For thepractical application of the CSM, we also developed a stan-dalone, coherent EUV light source based on high-order har-monic generation with a table-top, commercial Ti:sapphirelaser.Byinstallingthebeamstabilizationapparatus,thebeamfluctuationofthepumppulsebecomesmuchsmallerthantheradius of the 59th harmonic. Consequently, the utilizationefficiencyoftheEUVlightonthemaskwasdrasticallyimprovedwiththeusageofupgradedrelayoptics.Evendif-fractionpatternsofsmalldefects(onnm-scale) canbeobserved.TheresultsindicatethatHHG-CSMinspectionusingthediffractionpatterncanbotheff iciently andeffec-tively detect the existence of defects in the field of view, aswell as the fact that the 59th harmonic meets the spatialcoherencerequirementfortheCSM.Furthermore,thereconstruction of the complex image of the mask pattern wasalsodemonstratedusingthe59thharmonic.Thereconstructedimage quality resulting from the HHG-CSM was higher thanthat resulting from the SR-CSM, due to the improvement ofboth position accuracy and EUV light power. Thus, the state-of-the-artHHG-CSMwillundoubtedlybeapowerfultoolforEUV mask inspection in factories, such as mask shops andsemiconductorfabricationplants,aroundtheworld.

REFERENCES

[1] TerasawaT,YamaneT,TanakaT,SugaOandTomieT2010Actinicphasedefectdetectionforextremeultravioletlithographymaskwithabsorberpatterns Japan.J.Appl.Phys.4906GD02
[2] KwonHJ,Harris-JonesJ,TekiR,CordesA,NakajimaT,MochiI, GoldbergKA,YamaguchiYandKinoshitaH2011Printabilityofnativeblankdefectsandprogrammeddefectsandtheirstackstructures Proc.SPIE816681660H
[3] Mochi I, Goldberg K A, La Fontaine B, Tchikoulaeva A andHolfeld C 2010 Actinic

imaging of native and programmeddefectsonafull-fieldmaskProc.SPIE763676361A

[4] MochiI,GoldbergKA,XieR,YanP-YandYamazoeK2011Quantitativeevaluation ofmaskphasedefectsfromthrough-focusEUVaerialimagesProc.SPIE796979691X

[5] TchikoulaevaA,MiyaiH,SuzukiT,TakehisaK,KusunoseH,YamaneT,TerasawaT,WatanabeH,InoueSandMoriI2013EUVactinicblankinspection:fromprototypetoproductionProc.SPIE867986790I

[6] SuzukiT,MiyaiH,TakehisaK,KusunoseH,WatanabeHandMoriI2015DetectioncapabilityofActinicBlankInspectiontoolProc.SPIE965896580O

[7] HaradaT,NakasujiM,TadaM,NagataY,WatanabeTandKinoshitaH2011Criticaldimensionmeasurementofanextreme-ultravioletmaskutilizingcoherentextreme-ultravioletscatterometrymicroscopeatNewSUBARUJapan.J.Appl.Phys.5006GB03

[8] HaradaT,KishimotoJ,WatanabeTandKinoshitaH2009Maskobservationresultsusingacoherentextremeultravioletscatteringmicroscopeat NewSUBARUJ.Vac.Sci.Technol.B273203–7

[9] HaradaT,NakasujiM,KimuraT,WatanabeTandKinoshitaH2011Imagingofextreme-ultravioletmaskpatternsusingcoherentextreme-ultravioletscatterometrymicroscopebasedoncoherentdiffractionimagingJ.Vac.Sci.Technol.B2906F503

[10] HaradaT,NakasujiM,NagataY,WatanabeTandKinoshitaH2013Phaseimagingofextreme-ultravioletmaskusingcoherentextreme-ultravioletscatterometrymicroscopeJapan.J.Appl.Phys.5206GB02

[11] HaradaT,NakasujiM,NagataY,WatanabeTandKinoshitaH2013PhaseimagingofEUVmasksusingalenslessEUVmicroscopeProc.SPIE8701870119

[12] SeabergMD,ZhangB,GardnerDF,ShanblattER,MurnaneMM,KapteynHCandAdamsDE2014TabletopnanometerextremeultravioletimaginginanextendedreflectionmodeusingcoherentFresnelptychographyOptica139–44

[13] MiaoJ,SayreDandChapmanHN1998PhaseretrievalfromthemagnitudeoftheFouriertransformsofnonperiodicobjectsJ.Opt.Soc.Am.A151662–9

[14] MiaoJ,CharalambousP,KirzJandSayreD1999 Extendingthemethodologyofx-raycrystallographytoallowimagingofmicrometre-sizednon-crystallinespecimensNature400342–4

[15] MiaoJ,IshikawaT,AndersonEHandHodgson KO2003Phase retrieval of diffraction patterns from noncrystallinesamples using the oversampling method Phys. Rev. B 67174104

[16] HaradaT,TanakaY,WatanabeTandKinoshita H2013Phasedefectcharacterizationonanextreme-ultravioletblankmaskusingmicrocoherentextreme-ultravioletscatterometrymicroscopeJ.Vac.Sci.Technol.B3106F605

[17] TanakaY,HaradaT,AmanoT,UsuiY,WatanabeTandKinoshitaH2014Characterizationofsmallphasedefectsusingamicro-coherentextremeultravioletscatterometrymicroscopeJapan.J.Appl.Phys.

[18] Harada T, Hashimoto H, Tanaka Y, Amano T, Watanabe T and Kinoshita H 2015 Quantitative phase imaging of a small phase structure on an extreme-ultraviolet mask by coherent diffraction imaging

[19] Harada T, Hashimoto H, Amano T, Kinoshita H and Watanabe T 2016 Actual defect observation results of anextreme-ultraviolet blank mask by coherent diffractionimaging App.